DISCLAIMER

This report was prepared as an account of work sponsored by an agency of the United States Government. Neither the United States Government nor any agency thereof, nor any of their employees, makes any warranty, express or implied, or assumes any legal liability or responsibility for the accuracy, completeness, or usefulness of any information, apparatus, product, or process disclosed, or represents that its use would not infringe privately owned rights. Reference herein to any specific commercial product, process, or service by trade name, trademark, manufacturer, or otherwise does not necessarily constitute or imply its endorsement, recommendation, or favoring by the United States Government or any agency thereof. The views and opinions of authors expressed herein do not necessarily state or reflect those of the United States Government or any agency thereof. Reference herein to any social initiative (including but not limited to Diversity, Equity, and Inclusion (DEI); Community Benefits Plans (CBP); Justice 40; etc.) is made by the Author independent of any current requirement by the United States Government and does not constitute or imply endorsement, recommendation, or support by the United States Government or any agency thereof.

A DOE Energy Innovation Hub

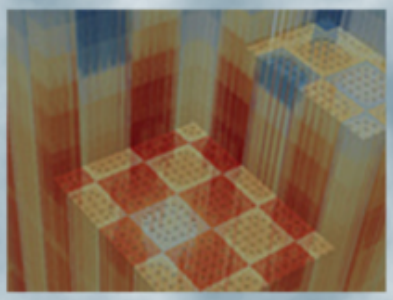

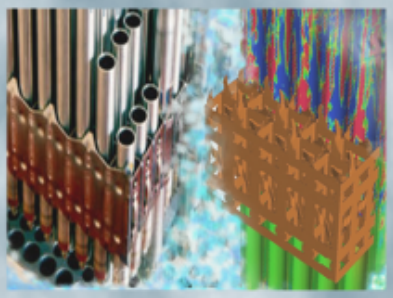

CRUD Source Term Assessment and Development for VERA

Alicia M. Elliott[1],
Benjamin Collins[1], David Andersson[2],
and Michael Short[3]

[1]Oak Ridge National Laboratory
[2]Los Alamos National Laboratory
[3]Massachusetts Institute of Technology

Milestone L3:FMC.CRUD.P19.04
April 30, 2019

U.S. DEPARTMENT OF ENERGY | Nuclear Energy

CONTENTS

1. INTRODUCTION

1.1. PRIMARY SIDE CORROSION IN PRESSURIZED WATER REACTORS

In pressurized water reactors, corrosion of primary loop materials is an ongoing process, as primary loop components (steam generator, hot leg, cold leg, and core) are constantly exposed to the coolant. As a result of this corrosion, primary loop materials are released into the coolant in the form of aqueous metal ions and particulate oxides. These corrosion products are the source of materials that form crud deposits on fuel rod clad surfaces.

The mass of corrosion products available to create crud will limit the rate and extent of crud buildup that occurs. This is commonly referred to as the crud "source term". The major contribution to the source term mass comes from the steam generator, due to the large surface area exposed to the coolant. Steam generators are not identical; the wetted area exposed to the coolant and the alloy used in the steam generator tubes vary. Different alloys corrode at different rates; Inconel 690 corrodes at approximately one-third of the rate of corrosion of Inconel 600 [1]. The mass of corrosion products released from the steam generator also varies by the area exposed to the coolant. The release of these corrosion products depends on the local environmental factors within the primary loop, including temperature, pH, local fluid conditions, electrochemical potential, and thermodynamic solubilities of the species present within this system. As such, each PWR will have a different crud source term based on these plant-specific parameters.

In order to accurately model and predict crud growth and issues that arise from the presence of crud (CIPS, CILC), the source of these corrosion product materials must be accurately modeled in a system mass balance. These models should be mechanistic, representative of the underlying physics phenomena, and account for the effects of the plant-specific design and operating parameters, including the alloys used, local temperatures, and fluid flow conditions.

1.2. THE CRUD "LIFE CYCLE"

One way to understand the relationship between ex-core corrosion and in-core crud is to consider the "life cycle" of the mass that eventually deposits on fuel rod cladding in the form of crud. Steam generator oxides form a two-layer structure, consisting of a compact inner oxide layer and a loose, particulate-based outer oxide layer. The physicochemical steps that lead to this dual-layer formation are more easily understood when considering the mass balance with a "life cycle" approach.

The crud "life cycle" (see Fig. 1) generally has 5 steps:

1. Base metal corrodes to form inner oxide layer (corrosion growth)
2. Ions are transported from base metal to coolant through inner oxide (corrosion release)
3. Particulates form on inner oxide surface by precipitating from solubles to form outer oxide
4. Particulates enter coolant due to erosion of outer oxide/crud
5. Coolant particulates deposit on fuel as crud

Each of these processes should be present in a comprehensive crud source term model to accurately model the underlying physics. The fifth process is already represented in MAMBA; the remaining 4 are discussed in this report.

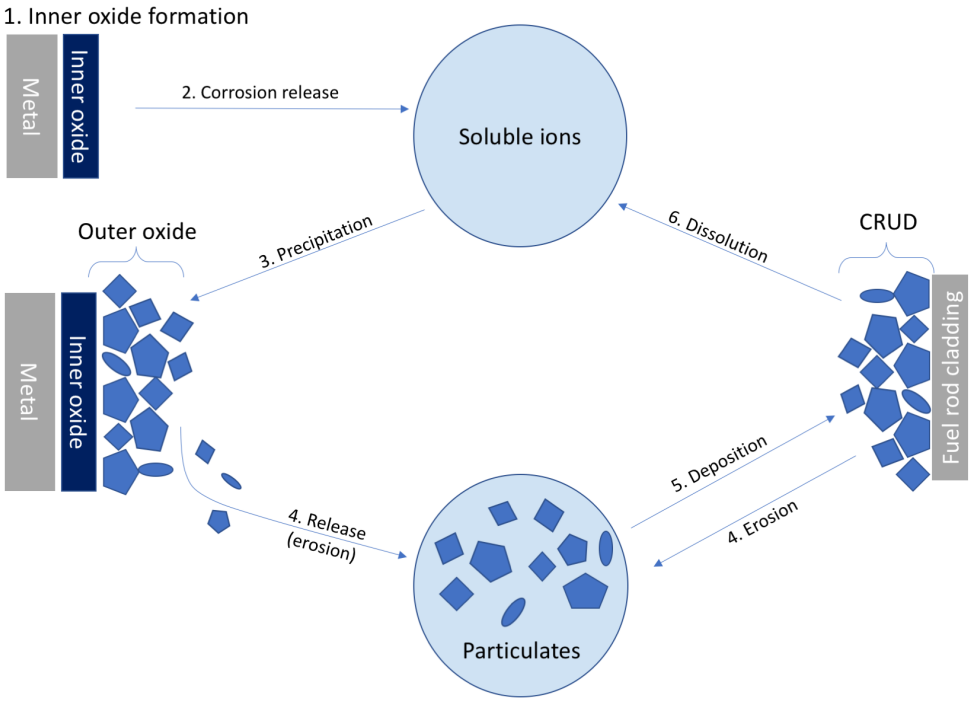

Figure 1. Simplified cycle of crud.

Dissolution of crud into soluble ions (represented in Fig. 1 as step 6) is thermodynamically possible at certain coolant conditions. However, this is not believed to contribute significantly to the crud source term and so was not included in this model [2]. Future modifications to the source term model might implement this step in order to have a more complete representation of the thermochemistry and physics governing the stability of PWR oxides.

2. INSIGHTS FROM OPEN LITERATURE

2.1. INNER OXIDE CORROSION GROWTH MECHANISM

The inner oxide layer contains two oxide phases: some Cr_2O_3 at the oxide-alloy interface with the bulk of the inner oxide containing $(Fe,Cr,Ni)_3O_4$ [3]. The model previously implemented in MAMBA assumes that the rate-limiting step for corrosion growth is outward diffusion of metal ions along inner oxide grain boundaries. However, recent studies have different conclusions on the corrosion mechanism for A690 oxidation in PWR primary water conditions, suggesting that the mechanism for inner oxide growth is inward diffusion of oxygen along grain boundaries (short-circuit diffusion paths) [3,4]. Supporting data can be found in Appendix 6.1.1.

There is some recent evidence suggesting that the inner oxide layer may not be completely passivating, as the chromia "layer" at the oxide-alloy interface is non-compact, and that the presence of surface defects on the alloy could possibly lead to a denser chromia layer which may be more passivating [3,4]. Supporting data can be found in Appendix 6.1.2.

2.2. OUTER OXIDE: COUPLING OF PARTICULATES AND SOLUBLES

The inner oxide layer grows due to corrosion of the base alloy. The outer oxide layer, however, precipitates. The particulate coolant concentration varies based upon the soluble concentration in the coolant, which couples the soluble and particulate species in the mass balance. If there is insufficient soluble species (i.e. coolant is not saturated), particulates will not form. The particulates are the dominant source term to the crud; however, the solubles are the source term to the particulates due to the nature of the oxidation/corrosion and precipitation process that creates the particulate oxides in the dual layer oxide [5]. Supporting data can be found in Appendix 6.1.3.

2.3. NICKEL METAL AND NICKEL OXIDE

According to EPRI reports, dissolved H_2 in coolant determines whether Ni metal or NiO is the thermodynamically stable solid to maintain equilibrium with aqueous Ni [6,7]. In regions with low concentrations of dissolved H_2, NiO is stable, whereas higher dissolved H_2 levels yield Ni metal as the stable species. This makes for an interesting effect in the core: boiling inside the crud layer locally depletes dissolved H_2, which makes NiO the stable species within the crud layer. However, bulk coolant dissolved H_2 levels are higher and thus Ni metal is stable outside of the crud layer. This could potentially have very interesting implications for this modeling effort and for physics as a whole.

2.4. EPRI MODEL (BOA)

EPRI's crud chemistry code, Boron-induced Offset Anomaly (BOA), is used to assess CIPS and CILC risk in PWRs [8]. Plant prediction capabilities present in BOA include [5]:

1. Soluble Ni, Fe levels in coolant
2. Particulate Ni, Fe levels in coolant
3. Ni release on shutdown
4. Ni/Fe ratio in fuel crud
5. Relative amounts of Ni metal on core, ex-core surfaces
6. Observed crud thicknesses
7. Amount of boron uptake in the crud

BOA was primarily designed to conservatively assess the risk of AOA in cycle core designs based on the predicted total core boron mass, the total crud mass in the core, and the maximum crud thickness. In order to predict the AOA risk of future cycles for a plant, at least two cycles should be modeled whose behavior is known to adjust the steam generator release rate and the crud carryover mass to match the actual behavior observed at that specific plant [9].

2.4.1 Equations for mass transport in primary circuit

The mass balance models implemented in BOA have been described in [5]. Steady state equation for moles of iron, nickel in the coolant in section i of primary circuit [5]:

$$\frac{\dot{m}}{\rho_{f,i-1}} C_{i-1} x_{i-1} - \frac{\dot{m}}{\rho_{f,i}} C_i x_i - J_i A_i = 0 \tag{1}$$

$\dot{m}$ = mass flow rate;
C_i = total molar concentration of coolant;
x = mole fraction of Ni or Fe in bulk coolant;
ρ_f = bulk density of water; A = section area;
J_i = molar flux of iron or nickel to/from the surface of the section

Multiple terms are needed for J_i to represent the multiple processes going on. The following subsections describe each of these terms and processes. It is assumed that the bulk coolant soluble concentrations are consistent throughout the loop due to high flow rates.

Soluble mass transport in solution

$$J = C_b \left[x_b u + k_m \left(x_b - x_s \right) \right] \tag{2}$$

C_b = total molar concentration in bulk;
x_b, x_s = mole fractions of Fe, Ni in bulk, at surface;

u = boiling velocity;
k_m = turbulent mass transfer coefficient.

This flux represents the transport of solubles from surface to the bulk coolant (and vice versa) due to boiling and turbulent fluid perturbations.

Soluble corrosion release

$$J_r = a\dot{m}_c \tag{3}$$

a = fraction of corrosion process released into coolant as Fe, Ni;
$\dot{m}_c$ = local corrosion rate.

a is a function of alloy composition and oxide phases present in the inner oxide, which is not detailed in published work. "The excess alloy passes through the inner oxide to the inner oxide/water interface where it can either precipitate out or pass into solution as soluble material. The release flux [...] equates to this excess metal but the particular amounts of Ni and Fe that are released depend on the assumed inner oxide structure" [5]. The local corrosion rate mechanism or mathematical representation is not discussed in the cited paper.

Soluble precipitation (to form particulates of Ni metal, NiO, and $Ni_xFe_{3-x}O_4$)

$$J_{p,\mathrm{Ni}}^{\mathrm{Ni}} = C_s k_a \left(x_{s,\mathrm{Ni}} - p\mathrm{Ni}\right) \tag{4}$$

C_s = total molar concentration at the surface;
k_a = precipitation rate constant for that solid;
$x_{s,\mathrm{Ni}}$ = mole fraction of nickel at surface;
pNi = precipitation parameter determined by equilibrium thermodynamics.
MAMBA uses an equation of the same form as Eqn. 4 used to fill crud pores from solubles precipitating.

$$R_{\mathrm{Precip}} = k_{\mathrm{Precipitate}}\eta\left(C_{\mathrm{Soluble}} - p_{\mathrm{Solid}}C_{\mathrm{coolant}}\right) \tag{5}$$

$k_{\mathrm{Precipitate}}$ is a precipitation rate constant (user defined) with an assumed Arrhenius temperature dependence. η is the crud porosity, p_{solid} is a precipitation parameter/condition for the solid from solubles, and C_{coolant} is the total molar concentration of the coolant.

Particulate deposition/release

$$J_{pa} = \rho_f x_{pa}\left(k_d + u\right) - k_r M \tag{6}$$

x_{pa} = weight fraction of nickel or iron particulate;
k_d, k_r = particulate deposition rate, release rate;
M = total amount of particulate on surface (outer oxide or fuel crud).

In Eqn. 6, k_d, k_r are constrained by plant observations and are currently the most challenging piece to address for this model. However, adding such a model to MAMBA would likely present a

significant improvement over not accounting for particulate formation/transport at all, as it would encapsulate more of the physics of the crud source term.

2.5. OTHER TAKEAWAYS

- Corrosion growth and corrosion release are separate processes; they have a similar mechanism, but with different species and different rates.
  - Corrosion growth is rate-limited by inwards oxygen diffusion along inner oxide grain boundaries.
  - Corrosion release of soluble ions is rate-limited by outwards metal ion diffusion along inner oxide grain boundaries.
- NiO and $NiFe_2O_4$ on boiling surfaces should be carried over from cycle to cycle (increasing the source term), but nickel metal should redissolve [5].
- The ratio of Ni:Fe in crud can be calculated by looking at NiO and $NiFe_2O_4$ deposit ratios [5]. This could be compared to plant crud scrape data to verify physics behavior.
- Effect of pH_T on corrosion and release rates are not significant because it affects precipitation due to solubility changes, not corrosion release.
- Nickel metal and nickel oxide particulates should be added to the MAMBA model; formation from solubles to outer oxide, release/erosion from outer oxide, deposition in crud, and also dissolution depending on thermodynamic stability locally. This would also allow calculation of ratios of NiO to $NiFe_2O_4$, a feature included in BOA that could be used to validate the models against crud scrape data from some plants.

3. CORROSION MODELS FOR VERA

3.1. CORROSION GROWTH OF INNER OXIDE

The new corrosion growth model for MAMBA assumes parabolic thick film growth kinetics, as was assumed in the previous model. Parabolic growth kinetic laws are represented with the following type of expression:

$$x^2 = E \cdot t \tag{7}$$

where x is the film thickness at time t, and E is a constant. Rearranging this slightly yields a direct expression for the thickness:

$$x(t) = \sqrt{E}\sqrt{t} \tag{8}$$

Note that $\sqrt{E}$ is still just a constant term, which we can call k. In order to get units of length from this calculation, the units of k must include length in the numerator and a square root of time in the denominator.

Corrosion rate constants for Alloy 600, 690, and SS 304 have been experimentally measured and reported in the open literature by Ziemniak and Hanson, Guinard, and Castelli [10–13]. These corrosion rate constants, denoted as k_p, have units of $\mathrm{mg/dm^2} - \sqrt{\mathrm{hr}}$. These rate constants are for the corrosion growth rate in terms of mass per unit area (denoted as $w(t)$ below).

$$w(t) = k_p\sqrt{t} = \frac{\text{mass of oxide}}{\text{surface area}} \qquad \text{(units: mg/dm}^2\text{)} \tag{9}$$

$$\frac{\partial w}{\partial t} = \frac{1}{2}\frac{k_p}{\sqrt{t}} \tag{10}$$

To convert this expression to calculate the oxide thickness, this can be simply divided by the oxide density, ρ_{oxide}.

$$x(t) = \frac{k_p(T)\sqrt{t}}{\rho_{\text{oxide}}} \tag{11}$$

k_p has an Arrhenius temperature dependence, as in the previous model. The activation energy and prefactor are approximated using measured data at 260, 325, and 350 °C, and the rate constant is then scaled to the desired temperature. Note that this temperature dependence means that the oxide thickness throughout the steam generator will vary with the temperature profile.

The use of different rate constants reflects a decision to assume a different rate-limiting mechanism of corrosion oxide growth. The previous model assumes the limiting step is diffusion of metal ions outwards along inner oxide grain boundaries, which is reflected by the use of diffusivities in place of rate constants. The new model assumes the rate-limiting step is oxygen diffusion inwards to create the inner oxide layer. This also reflects the separation of the mechanisms of growth of the inner oxide and outer oxide layers, which is not present in the previous model (see Section 2). The previous source term model implemented in MAMBA assumes that the corrosion release rate is equal to the corrosion growth rate, which may not be an accurate assumption, especially considering the dual-layer structure of the steam generator oxides. EPRI reports, Castelli, and other literature

suggest that generally the release rate is some fraction of the corrosion rate (between 5 and 50 percent is suggested) [10].

3.2. CORROSION RELEASE OF SOLUBLES

Assume the mechanism is diffusion of metal ions along grain boundaries through the inner oxide, which leads to release of soluble ions to the coolant. There is a concentration gradient across the oxide thickness, with a "concentration" of $\rho_{alloy} \times wt\%(elem)$ at the inner oxide-alloy interface, and effectively zero concentration in coolant/at surface (because the soluble saturated concentration is on the order of ppb/ppm, it is assumed to be negligible).

$$R = \frac{D^{Ni}_{oxide,GB} \rho_{alloy} wt\%(elem)}{x(t)} \times A_{cell} \tag{12}$$

The diffusivity is a function of temperature, as is the thickness of the oxide layer, x(t) (temperature dependence of k_p). A_{cell} is the surface area of the mesh cell. The corrosion release rate, R, must be integrated over the entire surface area of the steam generator to obtain the total release rate at a given state point.

4. PARTICULATE PHYSICS

As was discussed in Section 2, particulates form the second or outer layer of the oxide by precipitation of soluble ions from the coolant onto the surface of corrosion oxides.

Particulate formation is a multi-step process; local thermodynamic conditions must favor precipitation, including a sufficient supersaturation of nickel/iron ions near the surface (where there are inevitably heterogeneous nucleation sites to induce particulate precipitation). When a particle cluster initially forms (with only a few ions), it will not be stable unless it gains additional ions until it reaches the "critical size" for a stable nucleus in the current coolant conditions [14]. There might also be a chemical reaction associated with the reaction instead of physical processes to create the cluster (physisorption, adsorption), for e.g.

$$Ni^{2+}(aq) + 2\,Fe^{3+}(aq) + 4\,H_2O \longrightarrow NiFe_2O_4 + 6\,H^+ + H_2(aq) \qquad \text{(R-1)}$$

The Gibbs energy change of the system for this reaction will determine whether or not particulates will nucleate and grow to a stable minimum particle size. Note that this is minimum stable size; actual size can be larger, for highly supersaturated solution it will certainly be larger. Particle size depends on local flow rate, saturation concentrations, and the amount of time a particle remains on the steam generator surface before it is eroded off to the coolant. For this version of the model, precipitation of particulates is dependent on whether or not critical size nuclei can form based on this thermodynamic stability calculation.

4.1. PARTICLE THERMODYNAMIC STABILITY

Particulate nucleation requires the formation of a new surface; there is a thermodynamic energy penalty associated with surfaces, known as the surface energy (γ). In order for a particle to be energetically favorable and stable, the free energy "benefit" from the creation of a new volume (ΔG_V) must be greater than the penalty of creating a new surface. This energy balance is demonstrated in Eqn. 13 for a particle with volume V_p and surface area A_p.

$$G_{\text{particle}} = \Delta G_V V_p + \gamma A_p \qquad (13)$$

Thus, there is a critical particle size, based on the volume free energy, the surface energy, and the shape of the particle, above which the nucleated cluster will become thermodynamically stable. If the cluster does not reach this size, it will redissolve into the solution or shrink so that another stable particle can grow. This critical point will occur at $\frac{\partial G_{\text{particle}}}{\partial r} = 0$.

The following derivation will assume a spherical particle, though other particle geometries can be used as well by substituting in the appropriate expressions for particle volume and surface area into Eqn. 13. For a spherical particle, Eqn. 13 becomes:

$$G_{\text{particle}} = \frac{4}{3}\pi r_p^3 \Delta G_V + 4\pi r_p^2 \gamma$$

Differentiating with respect to the critical dimension (the radius, r_p), gives:

$$\frac{\partial G_{\text{particle}}}{\partial r} = 4\pi r_p^2 \Delta G_V + 8\pi r_p \gamma = 0$$

Rearranging the terms yields an expression for the critical radius as a function of the surface energy and the volume free energy:

$$\therefore r_{\text{crit}} = \frac{-2\gamma}{\Delta G_V} \tag{14}$$

Assume that the energy associated with forming a particle volume could be approximated as that of the chemical reaction forming the solid. The free energy change of a reaction can then be calculated based upon the chemical potentials of the reactants and products. This can then be used to calculate the approximate critical radius of stable particles using Eqn. 14.

The surface energy of formation for denuded (non-hydrated) stoichiometric (111) surfaces reported by Brenner is 1.71 J/m^2, and that for water-terminated (111) surfaces is 0.530 to 0.935 J/m^2 for 298.15 to 598.15 K [15, 16]. Based upon the calculated surface energies for multiple planes and surface terminations, the equilibrium particle geometry can be determined using a Wulff construction to minimize the surface energy contributions of the particle. An octahedral geometry was predicted by Brenner et al. with (111) surfaces contributing to most of the surface area of the particulate.

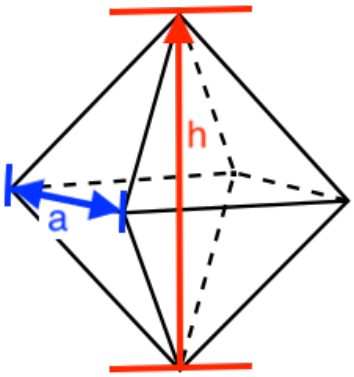

Figure 2. Geometry of octahedral particle; a is the edge length, h is the effective height.

Assuming an octahedral particle composed entirely of (111) surfaces with edge length a, Eqn. 14 can be rederived using the correct expressions for volume and surface area of this particle geometry:

$$G_{\text{particle}} = \frac{\sqrt{2}}{3}a^3\Delta G_V + 2\sqrt{3}a^2\gamma$$
$$\frac{\partial G_{\text{particle}}}{\partial r} = \sqrt{2}a^2\Delta G_V + 4\sqrt{3}a\gamma = 0$$

$$\therefore a_{\text{crit}} = \frac{-4\sqrt{3}\gamma}{\sqrt{2}\Delta G_V} \tag{15}$$

The volume free energy of formation of a $NiFe_2O_4$ particle can be determined based upon Reaction 1. The Gibbs energy of formation of $NiFe_2O_4$ can be calculated from the chemical potentials of all species in the reaction.

$$
\begin{aligned}
U = TS - PV + \sum \mu_i N_i \quad &\longrightarrow \quad dU = TdS - PdV + \sum \mu_i dN_i \\
G = U + PV - TS \quad &\longrightarrow \quad dG = dU + PdV + VdP - TdS - SdT \\
&\qquad = (TdS - PdV + \sum \mu_i dN_i) + PdV + VdP - TdS - SdT \\
&\therefore \; dG \qquad = \sum \mu_i dN_i + VdP - SdT
\end{aligned}
$$

Assuming a constant temperature and pressure system, this reduces to $dG = \sum \mu_i dN_i$. This can be used to determine the Gibbs free energy of formation of bulk nickel ferrite from Reaction 1.

$$
\begin{aligned}
\Delta G_{rxn} &= \sum_{i=\text{products}} \mu_i(T) dN_i - \sum_{j=\text{reactants}} \mu_j(T) dN_j \\
&= \Delta_f G^0_{NiFe_2O_4}(T) + \mu_{H_{2(aq)}}(T) + 6\mu_{H^+{}_{(aq)}}(T) - \mu_{Ni^{2+}{}_{(aq)}}(T) - 2\mu_{Fe^{2+}{}_{(aq)}}(T) - 4\mu_{H_2O}(T)
\end{aligned}
$$

The standard Gibbs free energy of formation for nickel ferrite between $298.15K \leq T \leq 898.15K$ was calculated using a correlation with experimentally determined fitting coefficients (see Fig. 3) reported by Brenner et al. [15]. The chemical potential of each species was calculated from the mole fraction of the species in solution using Eqn 16. The effective standard chemical potential ($\mu^0(T)$) was calculated using another correlation, see Fig. 4.

$$\mu_i(T) = \mu_i^0(T) + RT \ln(x_i) \tag{16}$$

To calculate the critical radius/edge length using Eqn. 14, the volume free energy should be converted from units of $\frac{\text{kJ}}{\text{mol}}$ to $\frac{\text{J}}{\text{cc}}$. To do this, simply multiply the free energy ΔG_{rxn} by $\frac{\rho_{NiFe_2O_4}}{MM_{NiFe_2O_4}} \times 1000$. The values used here are $\rho_{NiFe_2O_4} = 6.67$ g/cc and $\text{MM}_{NiFe_2O_4} = 234.38$ g/mol.

The number of moles of nickel in a single particle can be calculated based on the particle geometry. A single formula unit of $NiFe_2O_4$ will be 27% oxygen by mass, with the remaining 73% consisting of one-third nickel and two-thirds iron (roughly, as the masses of iron and nickel are approximately equivalent relative to oxygen).

$$n_{\text{Ni}} = \frac{1}{3}(0.73) V_p \frac{\rho_{NiFe_2O_4}}{MM_{\text{Ni}}} \tag{17}$$

The free energy of nucleating a critical particle calculated for typical PWR conditions is negative and large in magnitude (thus, particle formation is thermodynamically stable). Particle formation could be rate-limited by chemical reaction kinetics of particle formation, but given the low concentrations of nickel and iron ions in solution, it is more likely limited by the transport of ions to the surface where a particle can only form once there is a sufficient local supersaturation of nickel and iron ions. Additionally, as kinetic rates of reactions are difficult to measure, there is not an abundance of available data to determine this rate. Thus, it will be assumed that this system is transport-limited. It is also important to consider the timescales of interest: the smallest substeps of interest in MAMBA are on the order of hours to days, which are significantly larger than the timescales for transport of ions to the surface and likely larger than the kinetic rates for the chemical reactions of interest.

4.2. MASS TRANSFER IN A TURBULENT PIPE

Consider the transport of nickel ions from bulk solution to the pipe wall. The hydrated ions can be treated as spherical particles given the hydration radius (the radius of the ion plus the water molecules associated with it due to hydration/solvation). Fe^{2+} and Ni^{2+} hydrate with 6 H_2O molecules per ion. Literature reports hydrated radii of approximately 215 and 214-225 picometers, respectively [17, 18].

If the dynamic viscosity of the solution, μ, is known, the diffusivity of spherical particles in solution can be calculated using the Stokes-Einstein relation:

$$D_{\text{Stokes}} = \frac{k_b T}{6\pi r_{\text{hydr}} \mu} \tag{18}$$

It is important to note that the Stokes-Einstein relation applies in cases of low Reynolds number, which normally would not apply to this system. A better estimate would be to calculate a turbulent eddy diffusivity; however, assuming a laminar boundary layer near the surface, this approximation can be used in this model.

The Schmidt number represents the ratio of momentum diffusivity to mass diffusivity using the kinematic viscosity ν:

$$\text{Sc} = \frac{\nu}{D} \tag{19}$$

The Reynolds number can be calculated from the mass flux (G), hydraulic diameter(d_H), and viscosity:

$$\text{Re} = \frac{G d_H}{\mu} \tag{20}$$

The Sherwood number represents the ratio of convective mass transfer to diffusive mass transfer, and can be expressed from a correlation of the Reynolds number and Schmidt number:

$$\text{Sh} = 0.0288 \text{Re}^{4/5} \text{Sc}^{1/3} \tag{21}$$

Assuming the precipitation rate is limited by the transport of soluble species to the surface, the rate of transport of ions from the bulk coolant to the surface can be expressed by:

$$R_{\text{Precip}} = k_m \left(C_{bulk} - C_{surf} \right) \tag{22}$$

where k_m is the turbulent mass transfer coefficient calculated for aqueous/hydrated Ni, Fe ions, C_{bulk} is the bulk coolant concentration, and C_{surf} is the coolant concentration near the pipe surface. C_{sat} is the saturated concentration for equilibrium between the particulate solid and the coolant solubles; it is assumed that the concentration at the surface is equal to the saturated concentration, as any excess should precipitate out on the surface as particulates, since the system is transport-limited. C_{sat} can be calculated from equilibrium electrochemistry, or can be set by the user as a constant value for simplification.

Source term models of Castelli and Macdonald appear to assume that the rate-limiting process for precipitation is transport of solubles to/from the surface, where precipitation will occur if the coolant is saturated locally [10, 19]. Assuming the precipitation rate is limited by the transport of

soluble species to the surface, the rate of transport of ions from the bulk coolant to the surface can be expressed by:

$$R_{\text{Precip}} = k_m \left(C_{surf} - C_{sat} \right) \tag{23}$$

where k_m is the turbulent mass transfer coefficient calculated for aqueous hydrated/solvated Ni, Fe ions, and C_{sat} is the saturated concentration for equilibrium between the particulate solid and the coolant solubles. C_{sat} can be calculated from equilibrium electrochemistry, or can be set by the user as a constant value for simplification.

The turbulent mass transfer coefficient of ions, k_m, can be calculated by:

$$k_m = \frac{\text{Sh} D}{d_H} \tag{24}$$

The diffusion/transport-limited nucleation rate, determined by the rate of ions arriving at the pipe wall, can be calculated by:

$$\dot{R} = \frac{k_m}{n_{\text{Ni}}} \left(C_{\text{Ni}} - C_{\text{sat}} \right) \tag{25}$$

where n_{Ni} is the number of moles of nickel in one particle (Eqn. 17). The units of this rate is moles of particles created per square meter per second. It is assumed that the concentration at the surface is equal to the saturated concentration, as any excess should precipitate out on the surface as particulates, since the system is transport-limited. This flux represents the transport of solubles from surface to the bulk coolant (and vice versa) due to boiling and turbulent fluid perturbations. The corrosion release term will contribute solubles to the surface concentration in the coolant, which are then either precipitated out as particulates or transported to the bulk.

4.3. DINOV: PARTICULATES STICKING PROBABILITY THEORY

Particulate release to the coolant occurs as a result of erosion of the outer oxide. Intuitively, we expect this behavior to be dependent on various flow conditions and particle/fluid characteristics. Dinov published a model for crud particle-wall interactions based on Gerassimov's modification of Beal's model for deposition of particles in turbulent flow on pipe walls [20, 21]. By balancing the particle transfer fluxes between the coolant, the wall, and a boundary layer between the wall and bulk coolant, Dinov derived an expression for an "erosion coefficient" and "release coefficient" to describe the relationships analytically in terms of the sticking probability, particle properties, and flow conditions. These expressions are also similar in form to other models, including the Westinghouse CORA-II model [22]. Dinov proposed a two-step mechanism for particle-wall interactions and developed an expression for a sticking probability, p, which includes both steps of the mechanism ($p = p_1 \cdot p_2$). The first is the probability of dehydrating a particle's surface, which is a thermally activated process. Dinov represents this with an Arrhenius expression:

$$p_1 = \exp(-E_a / RT) \tag{26}$$

where E_a is the activation energy for detaching water molecules from the outer layer of the particulate. Dinov cites a value for the activation energy for dehydration of a 1 micron magnetite particle (45-50 kJ/mol) [21], which is a function of the particle size.

The second step is a surface chemistry barrier [21]. This includes the effect of particulate-surface charge interactions, and the chemistry conditions locally is implemented using the pH. Dinov implemented this using an assumption/expression from Westinghouse for a linear relationship between pH and particulate fraction deposited [21, 22]. The final expression for the particulate sticking probability, including both mechanisms, is:

$$p = \begin{cases} \exp(-E_a/RT) & \text{for pH } \leq 5 \\ \exp(-E_a/RT)(-0.3\text{pH} + 2.5) & \text{for } 5 \leq \text{pH} \leq 8 \\ \frac{1}{10}\exp(-E_a/RT) & \text{for pH } \geq 8 \end{cases} \tag{27}$$

The expressions derived for the erosion coefficient (k_e) and release constant (γ) are:

$$k_e = \frac{\gamma k_c}{k_c + p(v_B + v_f)} \tag{28}$$

$$\gamma = \frac{5 d_H}{\text{Re}\sqrt{f/2}} \tag{29}$$

where k_c is the turbulent mass transfer coefficient for particles, v_B is the velocity of particles due to Brownian motion, and v_f is the particle velocity due to momentum, which depends upon a particle stopping distance, S. The units of k_e are 1/seconds [21].

$$v_B = \sqrt{\frac{2k_b T}{m_p}} \tag{30}$$

$$v_f = \frac{u\sqrt{f/2}}{4}\left[0.05(r_p + S)\frac{u\sqrt{f/2}}{\nu}\right] \tag{31}$$

$$S = \frac{0.05u(d_p)^2\rho_p\sqrt{f/2}}{\mu} + \frac{d_p}{2} \tag{32}$$

4.4. OVERVIEW OF PARTICULATE MASS BALANCE EQUATIONS

For this model, deposition due to turbulent diffusion, Brownian diffusion, and inertial impaction will be neglected for simplification. Only deposition due to crud growth processes (as represented in MAMBA currently) will be implemented in this iteration of the model. The erosion rate expression from Dinov will be used as the source term of particulates in the coolant/loss term of particulates on the wall. The source term for particulates on the wall is from precipitation of critical stable particulates from solubles at the wall. Thus, the mass balance for the wall particulates and coolant particulates can be written as:

$$\frac{dW}{dt} = \dot{R} - k_e W \tag{33}$$

$$\frac{dC_p}{dt} = k_e W \pm (\text{deposition/erosion in core}) \tag{34}$$

where $\dot{R}$ is defined in Eqn. 23.

This equation couples the soluble ions to the particulates, which make the most significant contribution to the crud source term. It is also assumed that all excess Ni in coolant will be removed as precipitates if the supersaturation is high enough to precipitate particulates.

5. SUMMARY OF CRUD "LIFE CYCLE" EQUATIONS

1. Base metal corrodes to form inner oxide layer (corrosion growth)

Thickness of inner oxide due to corrosion growth:

$$x(t) = \frac{k_p \sqrt{t}}{\rho_{\text{oxide}}}$$

2. Ions diffuse from base metal to coolant through inner oxide (corrosion release)

Corrosion release rate of soluble nickel:

$$\frac{dC_{\text{Ni}}}{dt} = \frac{D^{Ni}_{oxide,GB} \rho_{alloy} wt\%(elem)}{x(t)} \times SA$$

3. Particulates form on inner oxide surface by precipitating from solubles

Stable particle formation rate:

$$\dot{R} = \frac{k_m}{d_H} \lfloor C_{\text{Ni}} - C_{\text{sat}} \rfloor$$

$$n_{\text{Ni}} = \frac{1}{3}(0.73)\frac{\sqrt{2}}{3} a^3 \frac{\rho_{\text{NiFe}_2\text{O}_4}}{MM_{\text{Ni}}}$$

$$a_{\text{crit}} = \frac{-4\sqrt{3}}{\sqrt{2}} \frac{\gamma}{\Delta G_{rxn}}$$

$$\Delta G_{rxn} = f(T, pH, x_{\text{Ni}}, x_{\text{Fe}}, x_{\text{Li}}, x_{\text{B}}, V_{\text{H}_2})$$

4. Particulates enter coolant due to erosion of outer oxide

Mass balance of particulates on wall and in coolant (excluding core deposition/erosion):

$$\frac{dW}{dt} = \dot{R} - k_e W$$
$$\frac{dC_p}{dt} = k_e W$$

Erosion/release coefficients:

$$k_e = \frac{\gamma k_c}{k_c + p(v_B + v_f)}$$
$$\gamma = \frac{5 d_H}{\text{Re}\sqrt{f/2}}$$

Brownian velocity, momentum velocity, particle stopping distance:

$$v_B = \sqrt{\frac{2k_bT}{m_p}}$$
$$v_f = \frac{u\sqrt{f/2}}{4}\left[0.05(r_p + S)\frac{u\sqrt{f/2}}{\nu}\right]$$
$$S = \frac{0.05u(d_p)^2\rho_p\sqrt{f/2}}{\mu} + \frac{d_p}{2}$$

Particulate sticking probability:

$$p = \begin{cases} \exp(-E_a/RT) & \text{for pH } \leq 5 \\ \exp(-E_a/RT)(-0.3\text{pH} + 2.5) & \text{for } 5 \leq \text{pH} \leq 8 \\ \frac{1}{10}\exp(-E_a/RT) & \text{for pH } \geq 8 \end{cases}$$

5. Coolant particulates deposit on fuel as crud
Already implemented in MAMBA.

REFERENCES

[1] D. Hussey, "Open Literature Discussion of PWR Source Term Modeling for CIPS/CILC," *CASL Crud Workshop*, 2015.

[2] M. Short, "The particulate nature of the crud source term in light water reactors," *Journal of Nuclear Materials*, **509**, pp. 478–481 (2018).

[3] W. Kuang, M. Song, P. Wang, and G. S. Was, "The oxidation of alloy 690 in simulated pressurized water reactor primary water," *Corrosion Science*, **126**, pp. 227–237 (2017).

[4] L. Marchetti, S. Perrin, F. Jambon, and M. Pijolat, "Corrosion of nickel-base alloys in primary medium of pressurized water reactors: New insights on the oxide growth mechanisms and kinetic modelling," *Corrosion Science*, **102**, pp. 24–35 (2016).

[5] J. Deshon et al., "Recent Development of BOA Version 3," *International Conference on Water Chemistry of Nuclear Reactor Systems*, October 3-7, 2010.

[6] "Behavior of Nickel/Nickel Oxide in PWR Environments," 1001397, EPRI (2001).

[7] "Impact of Nickel Oxide Solubility on Pressurized Water Reactor Fuel Deposit Chemistry," 1003155, EPRI (2002).

[8] EPRI, *Boron-induced Offset Anomaly (BOA) Risk Assessment Tool, Version 3.0*, EPRI, Palo Alto, CA, 2010.

[9] "PWR Axial Offset Anomaly (AOA) Guidelines, Revision 1," 10808102, EPRI (2004).

[10] R. Castelli, *Nuclear Corrosion Modeling: The Nature of CRUD*, Butterworth-Heinemann (2009).

[11] S. E. Ziemniak and M. Hanson, "Corrosion behavior of NiCrFe Alloy 600 in high temperature, hydrogenated water," *Corrosion Science*, **48**, *2*, pp. 498–521 (2006).

[12] L. Guinard, O. Kerrec, D. Noel, S. Gardey, and F. Coulet, "Influence of the initial surface condition on the release of nickel alloys in the primary circuit of PWRs," EDF–97-NB-00045, EDF (1997).

[13] S. Ziemniak and M. Hanson, "Corrosion Behavior of 304 Stainless Steel in High Temperature, Hydrogenated Water," (2001).

[14] R. W. Balluffi, S. M. Allen, and W. C. Carter, *Kinetics of Materials*, John Wiley & Sons (2005).

[15] C. J. O'Brien, Z. Rák, and D. W. Brenner, "Free energies of (Co, Fe, Ni, Zn)Fe2O4spinels and oxides in water at high temperatures and pressure from density functional theory: results for stoichiometric NiO and NiFe2O4surfaces," *Journal of Physics: Condensed Matter*, **25**, *44*, pp. 445008 (2013).

[16] C. J. O'Brien, Z. Rák, and D. W. Brenner, "Calculated Stability and Structure of Nickel Ferrite Crystal Surfaces in Hydrothermal Environments," *The Journal of Physical Chemistry C*, **118**, *10*, pp. 5414–5423 (2014).

[17] Y. Inada, A. M. Mohammed, H. H. Loeffler, and B. M. Rode, "Hydration Structure and Water Exchange Reaction of Nickel(II) Ion: Classical and QM/MM Simulations," *The Journal of Physical Chemistry A*, **106**, *29*, pp. 6783–6791 (2002).

[18] T. Remsungnen and B. M. Rode, "Molecular dynamics simulation of the hydration of transition metal ions: the role of non-additive effects in the hydration shells of Fe2 and Fe3 ions," *Chemical Physics Letters*, **385**, *5-6*, pp. 491–497 (2004).

[19] D. D. Macdonald et al., "Electrochemistry of Water-Cooled Nuclear Reactors," *Nuclear Energy Education Research (NEER) Final Technical Progress Report* (2006).

[20] S. K. Beal, "Deposition of Particles in Turbulent Flow on Channel or Pipe Walls," *Nuclear Science and Engineering*, **40**, *1*, pp. 1–11 (1970).

[21] K. Dinov, "A Model of Crud Particle/Wall Interaction and Deposition in a Pressurized Water Reactor Primary system," *Nuclear Technology*, **94**, pp. 281 – 285 (1991).

[22] "The CORA-II Model of PWR Corrosion Product Transport," EPRI NP-4246, EPRI (1985).

[23] D. H. Lister and W. G. Cook, "Chapter 14: Nuclear Plant Materials and Corrosion," *The Essential CANDU, A Textbook on the CANDU Nuclear Power Plant Technology*, ISBN 0-9730040, www.nuceng.ca/candu/, Accessed: 10/30/2018.

[24] C. O'Brien, Z. Rák, E. Bucholz, and D. Brenner, "First principles calculations predict stable 50 nm nickel ferrite particles in PWR coolant," *Journal of Nuclear Materials*, **454**, *1-3*, pp. 77–80 (2014).

[25] D. W. Brenner, S. Lu, C. J. O'Brien, E. W. Bucholz, and Z. Rak, "A particle assembly/constrained expansion (PACE) model for the formation and structure of porous metal oxide deposits on nuclear fuel rods in pressurized light water reactors," *Journal of Nuclear Materials*, **457**, pp. 209–212 (2015).

[26] S. Dickinson, J. Henshaw, J. McGurk, and H. Sims, "Modeling PWR Fuel Corrosion Product Deposition and Growth Process: Final Report," 1011743, EPRI (2005).

6. APPENDIX

6.1. SUPPORTING DATA FOR ASSUMPTIONS IN MODEL

6.1.1 Inner oxide growth mechanism

"Previous studies consistently suggest that the inner layer contains both spinel and corundum Cr_2O_3 which is at the oxide/substrate interface." [3]

"Tracer experiments by Marchetti et al. confiarmed that the formation of inner oxide mainly occurs via the inward diffusion of oxygen" [3].

"The inner oxide forms via inward diffusion of oxygen. When oxygen reaches the oxidation front, the potential is low, favoring the formation of Cr_2O_3 [...] The inner oxide layer is composed of Cr-rich $(Fe,Cr,Ni)_3O_4$ and chromia, and is mixed with un-oxidized metal. The compactness of the inner oxide decreases with depth into the oxide layer. Both $(Fe,Cr,Ni)_3O_4$ and chromia grow into the matrix in specific orientations with the matrix via solid-state reactions of the substrate with the inwards diffusing oxygen." [3]. "Discreet chromia forms first along the widely spaced lattice planes of the metal substrate at the oxidation front where the oxygen concentration is low. [...] Compact Cr_2O_3 layers cannot develop as there is no long-range outward diffusion of Cr in substrate with low defect density at low temperature. Further from the oxide-metal interface where the potential is higher, spinel becomes thermodynamically stable and starts to form among the preexisting non-compact chromia" [3].

"Both $(Fe,Cr,Ni)_3O_4$ and chromia have well defined crystallographic orientations with the substrate because they are products of solid state reactions between oxidant and substrate. [...] Spinel and substrate are both face centered cubic (FCC) and have cube-on-cube relationships, consistent with previous work. Cr_2O_3 has a hexagonal close packed (HCP) crystal structure. [...] The close packed lattice planes of chromia are well aligned with those of the substrate. Moreover, the high resolution images clearly show that the interfaces between matrix and chromia are semi-coherent. It is unlikely that fast diffusion along dislocations could result in such rigid crystal orientation relationships between oxides and substrate. More precisely, the chromia filaments form along the lattice planes of substrate with high packing densities, which supports the preferential diffusion of oxygen to maintain well-defined orientation relationships with the matrix, irrespective of the existence of dislocations" [3].

"Experiments involving gold markers and isotopically labelled oxygen have shown that the formation of the internal scale results from anionic diffusion along short-circuits network such as grain boundaries. [...] If anionic diffusion seems to be responsible for the growth of the internal oxide scale, the formation of the external one, as well as the release of cations into the primary fluid, need Fe and Ni diffusion through the internal layer. Considering semiconducting properties of both $Ni_{1-x}Fe_xCr_2O_4$ and Cr_2O_3, the diffusion of Fe and Ni cations takes place via interstitial sites, in the cation sublattices. As it has been shown that oxygen diffusion through the protective scale involves a short-circuits network, it is assumed that is also the case for cations diffusion." [4]

6.1.2 Inner oxide structure and corrosion resistance

"[...] the inner oxides consist of Cr-rich $(Fe,Cr,Ni)_3O_4$ and Cr_2O_3, consistent with previous work. Interestingly, the relative amount of $(Fe,Cr,Ni)_3O_4$ decreases as it moves further into the substrate, consistent with the EDS results which show that the contents of Ni and Fe decrease with distance to

the surface. [...] Cr_2O_3 penetrates deeper into the substrate because the oxygen potential decreases with depth and the range of potentials over which chromia exists extends to lower values than that of the spinel according to the Pourbaix diagrams up to 300 °C" [3]

"The internal part of the oxide scale is composed of a continuous layer of $Ni_{1-x}Fe_xCr_2O_4$ and of Cr_2O_3 nodules uniformly dispersed along the oxide/alloy interface.Contrary to what has been sometimes exhibited from oxygenated primary water exposures, TEM characterisations of the internal oxide scale formed during the immersion of Ni-base alloys to conventional PWR primary media (i.e. containing dissolved hydrogen) have not evidences any porosity in this scale. For that reason, all transport through the internal oxide scale is supposed to occur by solid state processes" [4].

"The compactness of the inner oxide decreases with depth into the oxide layer. [...] Further from the oxide-metal interface where the potential is higher, spinel becomes thermodynamically stable and starts to form among the preexisting non-compact chromia. Both $(Fe,Cr,Ni)_3O_4$ and chromia grow into the matrix in rigid orientations with the matrix via solid-state reactions" [3].

"The character of the inner layer is critical to the corrosion resistance of alloy 690 as it has been noted that a non-compact oxide layer is not protective. The surface state seems to play an important role in the formation of the inner layer. [...] the inner oxide was formed via the inward diffusion of oxygen without long range diffusion of Cr. [...] a higher defect density in the substrate surface layer can enhance the outward diffusion of Cr and promote formation of a denser and more protective Cr_2O_3 layer" [3].

6.1.3 Precipitation of particulates from solubles

"The outer-oxide layers are variants of the inverse spinel magnetite and are designated as $Ni_xFe_{3-x}O_4$; again, x depends on the composition of the underlying alloy but also, since the layer is precipitated from solution, it depends upon the metals dissolved in the coolant and originating in the rest of the circuit [Cook et al., 2000]" [23].

"In PWRs, the composition of the outer layers on the alloys approximates $Ni_{0.6}Fe_{2.4}O_4$, a variant of nickel ferrite (or trevorite, $NiFe_2O_4$). This also approximates the composition of the particulate matter (called "crud") that circulates in suspension in the primary coolant at concentrations of the order of a ppb (part per billion) or less and that forms deposits on in-core fuel assemblies" [23].

"It is generally accepted that the outer oxide particle on alloy 690 has a spinel structure and forms by the precipitation of cations dissolved in the solution, similar to that on alloy 600 and stainless steel." [3]

"The outer oxide particle contains mostly Fe and Ni with an atomic ratio of Fe to Ni close to 2, suggesting that the stoichiometry is $NiFe_2O_4$, and of spinel structure. The spinel grows by precipitation, and has a flexible range of metallic element composition which is dependent on chemical compositions of sample substrate, the corrosion potential and the materials used for the water loop and autoclave." [3]

"It has been shown that the formation of nickel ferrite crystals results from precipitation phenomena, because (i) they can appear on Fe-free alloy and (ii) the amount of $Ni_{1-z}Fe_{2+z}O_4$ formed depends on media saturation. The roles of substrate (i) sub-surface defects and (ii) crystalline orientation on the preferential location of ferrite crystals underline that their precipitation involves heterogeneous nucleation and growth processes" [4]

"The release of Fe and Ni cations in the primary medium, according to Reactions (14) and (15), may lead to local oversaturation at the vicinity of the medium/oxide interface. The formation

of metastable solid nickel and iron hydroxides on the oxidized surface probably results from precipitation of stable neutral aqueous complexes, such as in (17) and (18) [...] Once formed, these metastable hydroxides may diffuse on the surface towards preferential sites, where nucleation or growth of nickel ferrite crystals occurs (19)" [4]

Reactions 14, 15, 17, 18, 19:

$$\mathrm{Ni^{2+}_{(chromite)} + 2\,H_2O_{(adsorbed)} \rightleftharpoons Ni(OH)_{2(aq)} + 2\,H^+_{(aq)}}$$
$$\mathrm{Fe^{2+}_{(chromite)} + 2\,H_2O_{(adsorbed)} \rightleftharpoons Fe(OH)_{2(aq)} + 2\,H^+_{(aq)}}$$
$$\mathrm{Ni(OH)_{2(aq)} \rightleftharpoons \langle Ni(OH)_2 \rangle}$$
$$\mathrm{Fe(OH)_{2(aq)} \rightleftharpoons \langle Fe(OH)_2 \rangle}$$
$$\mathrm{(2+z)\langle Fe(OH)_2 \rangle + (1-z)\langle Ni(OH)2 \rangle \rightleftharpoons Ni_{1-z}Fe_{2+z}O_4 + 2\,H_2O + H_{2(aq)}}$$

[4]

6.2. CHEMICAL THERMODYNAMICS DATA FROM BRENNER ET AL

Table A.1. Coefficients for fitting the experimental standard Gibbs free energy of formation at 1 bar for use with (A.1).

Material	A (kJ mol^{-1})	B (kJ mol^{-1} K^{-1})	$C \times 10^{-3}$ (kJ mol^{-1})	$D \times 10^{-5}$ (kJ mol^{-1} K^{-2})	E (kJ K mol^{-1})	$F \times 10^{-6}$ (kJ mol^{-1} K^{-3})
Hematite[a]	−743.5230	−0.7602	153.5600	−11.2300	−7230.6900	
Magnetite[a]	−1017.4380	−1.0477	210.0790	−17.1050	−8742.8800	
Goethite[a]	−491.9690	−0.7379	149.0130	−9.9740	−7244.0800	
Nickel oxide[b]	−211.5957	−0.2089	43.6816	−2.7721	−2831.7975	
Nickel ferrite[c]	−974.4477	−1.0467	210.7760	−15.8693	−9587.1100	
Zinc oxide[d]	−320.5983	−0.0945	23.1149	−1.1366	−3654.6700	
Zinc ferrite[c]	−1073.6393	−0.8147	168.0127	−9.5030	−10 276.7981	
Cobalt oxide[a]	−794.8710	−1.0603	212.3490	−12.7792	−9946.2000	
Cobalt ferrite[c]	−992.3587	−1.0514	210.7773	−15.6596	−9141.3533	
Water (gas)[a]	−228.5820	−0.2041	38.7665	−3.3351	−651.0610	0.006 395 37
Water (liquid)[a]	−237.1410	−0.7437	146.2140	−18.0804	−3155.0600	

[a] JANAF [93];. [b] Pankratz [94];. [c] Barin [95];. [d] Knacke [96].

$$\Delta_f G^0\ (298.15\ \mathrm{K} \le T \le 898.15\ \mathrm{K}) \left[\frac{\mathrm{kJ}}{\mathrm{mol}}\right] = A + BT + CT\ln T + DT^2 + E\frac{1}{T} + FT^3.$$

Figure 3. The coefficients in this table are used in the equation shown to calculate the standard Gibbs energy of formation [15]

Brenner et al. determined the size of stable $NiFe_2O_4$ particles in PWR conditions using first-principles based thermodynamics calculations for surface free energies and bulk free energies of formation [15, 16, 24, 25]. These calculations predicted that 50 nm octahedral particles would be stable in typical PWR conditions. However, the molal concentrations of nickel ions and iron ions (1.66×10^{-14} mol/kg and 4.17×10^{-13} mol/kg, respectively) used appear to be orders of magnitude lower than those reported in plant data. This is roughly equivalent to 1×10^{-7} ppb for nickel ions. Plant measurement data from EPRI reported an average value of 164.43 ng/kg of soluble nickel, which should correspond to 2.8×10^{-9} mol/kg (approximately 0.164 ppb) [26]. The values used by Brenner et al. are significantly lower than the measured plant data for soluble nickel, which would alter the thermodynamic equilibrium calculation and yield a less thermodynamically stable case for $NiFe_2O_4$ particulates, particularly as these values are below the observed solubility limit of $NiFe_2O_4$ (0.03 to 0.1 ppb) [5]. As such, a method to determine the particle size and nucleation rate is presented in this report to calculate these parameters based upon the concentrations of soluble species, pH, T, and fluid parameters.

Table B.1. Effective standard state chemical potentials of the elements determined by the global fitting procedure. Standard state refers to the elements being in their equilibrium phase at the given temperature and pressure. The values are reported for a pressure of 1 bar.

Material	A (kJ mol^{-1})	B (kJ mol^{-1} K^{-1})	$C \times 10^{-3}$ (kJ mol^{-1})	$D \times 10^{-5}$ (kJ mol^{-1} K^{-2})	E (kJ K mol^{-1})	$F \times 10^{-7}$ (kJ mol^{-1} K^{-3})
Fe	−542.2234	−3.0562	579.0786	−137.5260	11 166.2402	4.6487
Ni	−281.4639	−1.9781	374.1096	−88.6994	7509.7748	2.9938
Zn	−54.9384	−1.9691	371.2403	−85.3290	7512.9363	2.7094
Co	−455.2552	−3.0522	578.3376	−138.9698	11 566.9879	4.6488
H_2	−707.8309	−1.7026	315.5267	−91.5869	13 267.8307	3.2427
O_2	−974.8047	5.1079	−973.6217	214.8372	−12 378.7410	−6.9730

Table B.2. Effective standard state chemical potentials of the aqueous compounds determined by the global fitting procedure. Standard state refers to the elements being in the ionization state indicated, at the given temperature and pressure. The values are reported for a pressure of 155 bar.

Material	A (kJ mol^{-1})	B (kJ mol^{-1} K^{-1})	$C \times 10^{-3}$ (kJ mol^{-1})	$D \times 10^{-5}$ (kJ mol^{-1} K^{-2})	E (kJ K mol^{-1})	$F \times 10^{-7}$ (kJ mol^{-1} K^{-3})
$(H_2O)_l$	−1432.1355	0.3236	−63.2328	1.7607	2795.8512	0.3236
$(H_2O)_g$	−1423.3658	3.0769	−61.2421	158.4713	−405.2578	−6.2195
$(Ni^{2+})_{aq}$	380.2174	−0.5261	117.7779	−32.0450	−6651.1741	2.8394
$(Fe^{2+})_{aq}$	73.6321	−2.0376	410.5225	−114.4011	−1180.3670	5.9501
$(Fe^{3+})_{aq}$	501.5834	1.7384	−325.9208	122.2772	−19 324.4212	−3.2589
$(Zn^{2+})_{aq}$	505.2433	−0.8511	186.2069	−58.5909	−6173.7389	3.8531
$(Co^{2+})_{aq}$	197.7945	−1.8542	373.2061	−101.3680	−1485.7017	5.2453
$(NiO)_{aq}$	−933.9167	1.1246	−221.3906	56.9659	−1164.4941	−2.2489
$(H_2)_{aq}$	−689.7183	3.0386	−614.1494	198.8776	−3884.0976	−9.9899
$(OH^-)_{aq}$	−1352.5976	−15.0713	3002.8552	−981.6527	42 677.6623	46.0577

$$\mu^0\,(298.15\ \mathrm{K} \le T \le 617.15\ \mathrm{K})\left[\frac{\mathrm{kJ}}{\mathrm{mol}}\right] = A + BT + CT\ln T + DT^2 + E\frac{1}{T} + FT^3.$$

Figure 4. The coefficients in this table are used in the equation shown to calculate the effective chemical potentials of aqueous species [15]